H1prelim-08-042 Submitted to

XVI International Workshop on Deep-Inelastic Scattering, DIS2008, April 7-11, 2008, London
Parallel Session **Structure Functions**

Electronic Access:https://www-h1.desy.de/publications/H1preliminary.short_list.html

A Measurement of the Longitudinal Proton Structure Function $F_L(x, Q^2)$ at high Q^2 at HERA

H1 Collaboration

Abstract

A measurement of the longitudinal proton structure function $F_L(x, Q^2)$ derived from inclusive deep inelastic ep scattering cross section measurements at high Q^2 with the H1 detector at HERA is presented. The data were taken in the year 2007 at a positron beam energy of $E_e = 27.5$ GeV and proton beam energies E_p of 920 GeV, 575 GeV and 460 GeV. The measurements of the NC cross sections from this analysis combined with the reported earlier NC cross section measurements for the same data periods at medium Q^2 allowed to measure $F_L(x, Q^2)$ in a range of high four-momentum transfer squared $12 \leq Q^2 \leq 800$ GeV^2 and correspondingly Bjorken-x between $0.00028 \leq x \leq 0.0353$. The measured longitudinal structure function is found to be consistent with the NLO QCD expectations.

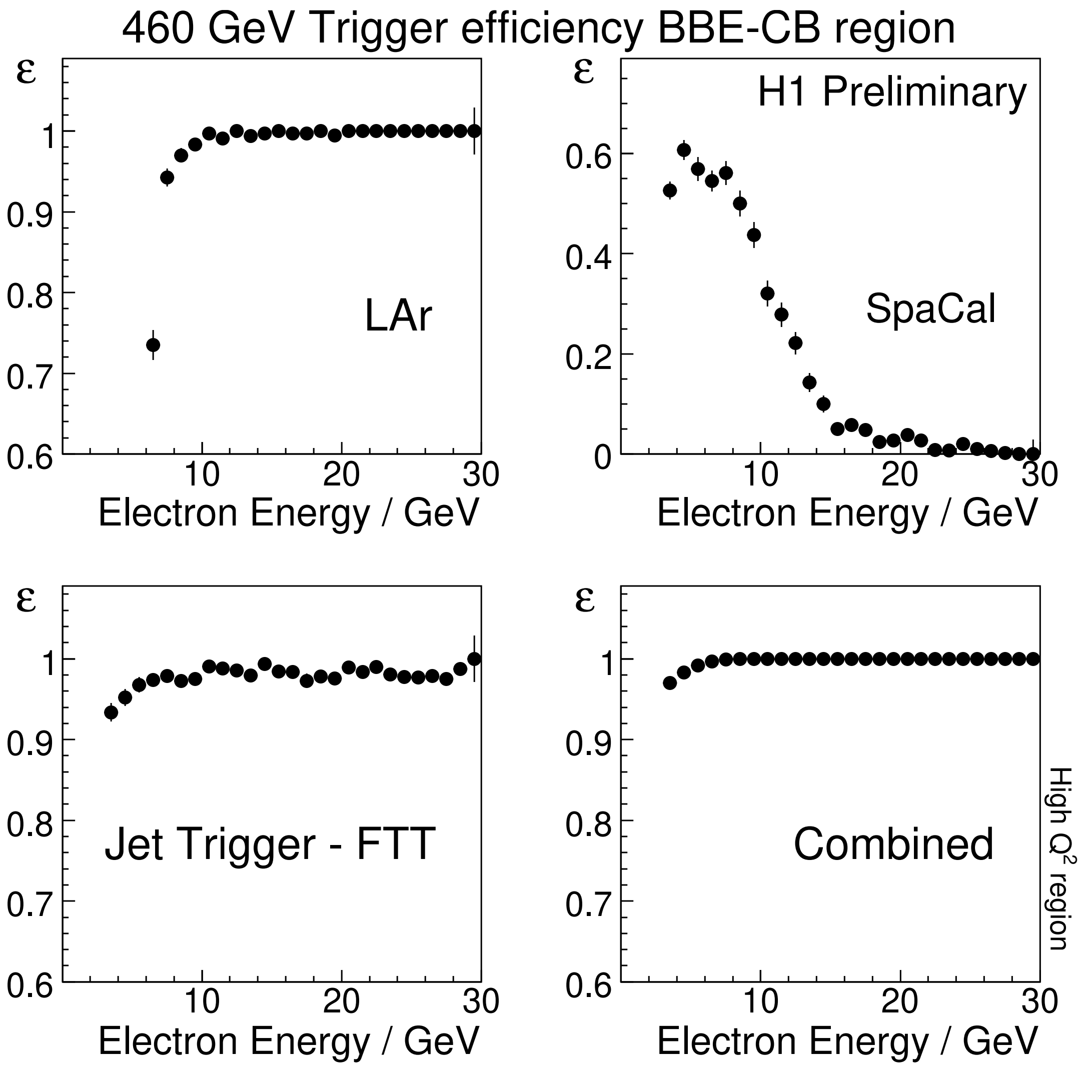

Figure 1: Example trigger efficiencies for the LAr, Spacal, Jet Trigger - FTT subtriggers as a function of the scattered electron energy, shown for electrons pointing to the transition BBE-CB region of the LAr calorimeter for the low proton beam energy (460 GeV). Combined trigger efficiency is shown in the bottom right plot.

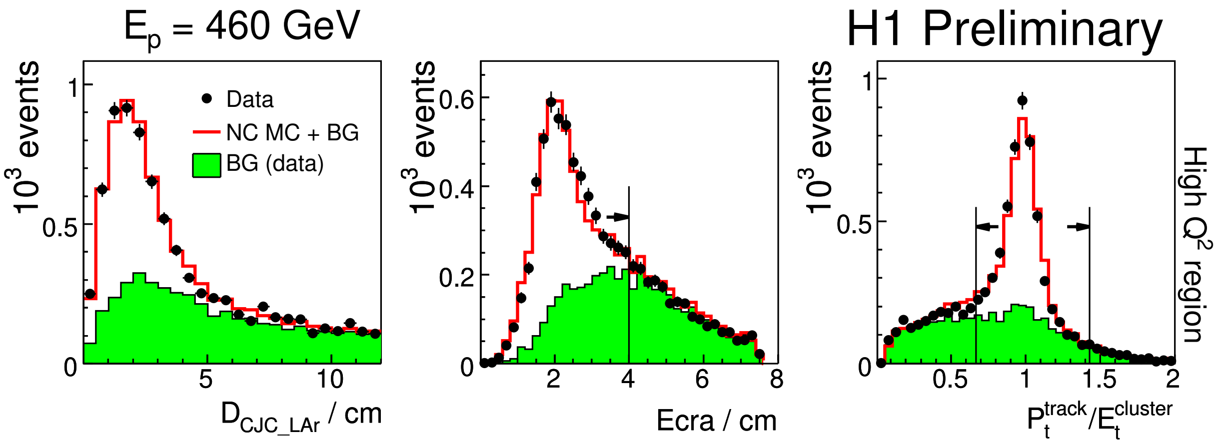

Figure 2: Comparison of the correct electron charge data (points) with a sum of background determined from the wrong "electron" charge data (green histogram) and DIS MC (open histogram) for the low proton beam energy (460 GeV) in the region of the electron energy below 6 GeV without applying addition electron identification cuts. The distributions from left to right are the distance between extrapolated track and the center of gravity of the cluster in LAr (D_{CJC_LAr}), tranverse size of the electron cluster in LAr (Ecra) and ratio of transverse momenta as measured in the tracker and in the LAr calorimeter ($Pt_{track}/Et_{cluster}$). The cut values on the two latter quantities applied in the analysis are indicated by vertical lines.

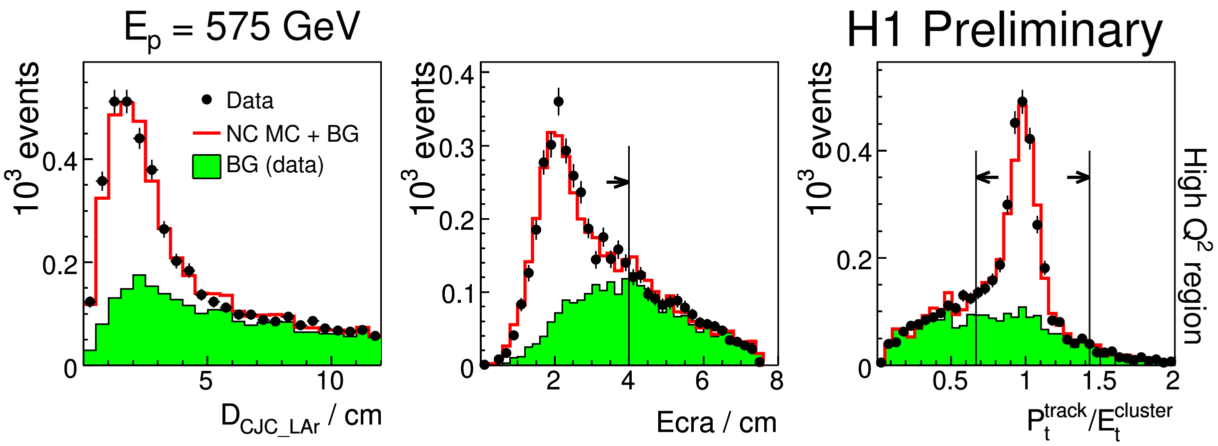

Figure 3: Comparison of the correct electron charge data (points) with a sum of background determined from the wrong "electron" charge data (green histogram) and DIS MC (open histogram) for the medium proton beam energy (575 GeV) in the region of the electron energy below 6 GeV without applying addition electron identification cuts. The distributions from left to right are the distance between extrapolated track and the center of gravity of the cluster in LAr (D_{CJC_LAr}), tranverse size of the electron cluster in LAr (Ecra) and ratio of transverse momenta as measured in the tracker and in the LAr calorimeter ($Pt_{track}/Et_{cluster}$). The cut values on the two latter quantities applied in the analysis are indicated by vertical lines.

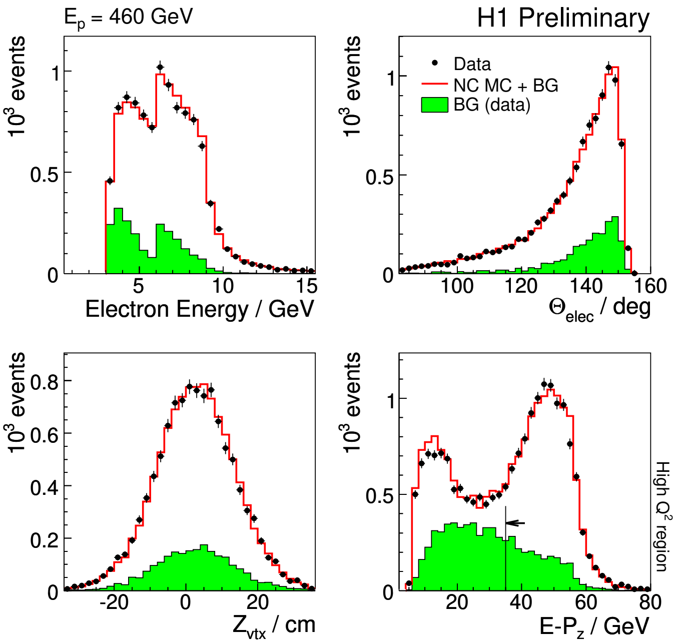

Figure 4: Comparison of the correct electron charge data (points) with a sum of background determined from the wrong "electron" charge data (green histogram) and DIS MC (open histogram) for the low proton beam energy (460 GeV) in the high y range $0.7 < y < 0.9$. The distributions from left to right and from top to bottom are the scattered electron energy, the scattered electron polar angle Θ_{elec}, the z-position of the event vertex Z_{vtx} and the sum $E - p_z$ of all final state particles. The vertical line in $E - p_z$ distribution indicates the cut value.

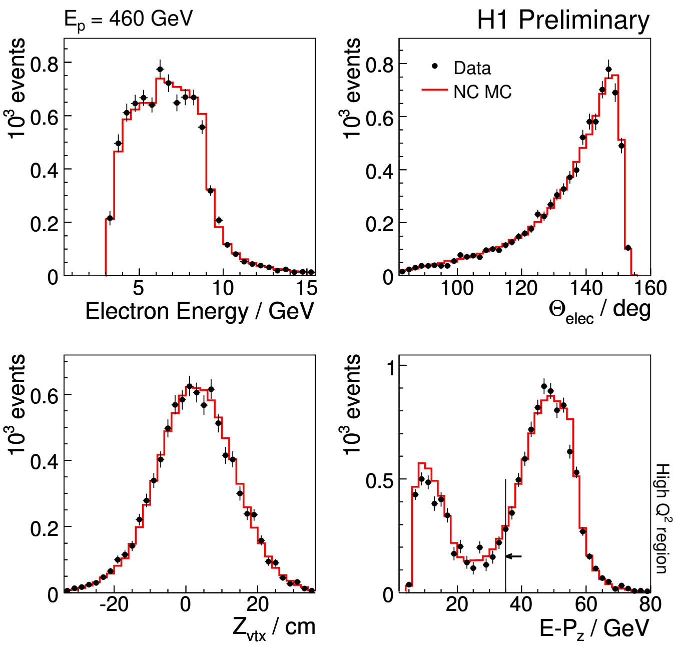

Figure 5: Comparison of signal distributions (background subtracted with corresponding asymmetry factor) for the low proton beam energy (460 GeV) in the high y range $0.7 < y < 0.9$. The distributions from left to right and from top to bottom are the scattered electron energy, the scattered electron polar angle Θ_{elec}, the z-position of the event vertex Z_{vtx} and the sum $E - p_z$ of all final state particles. The vertical line in $E - p_z$ distribution indicates the cut value.

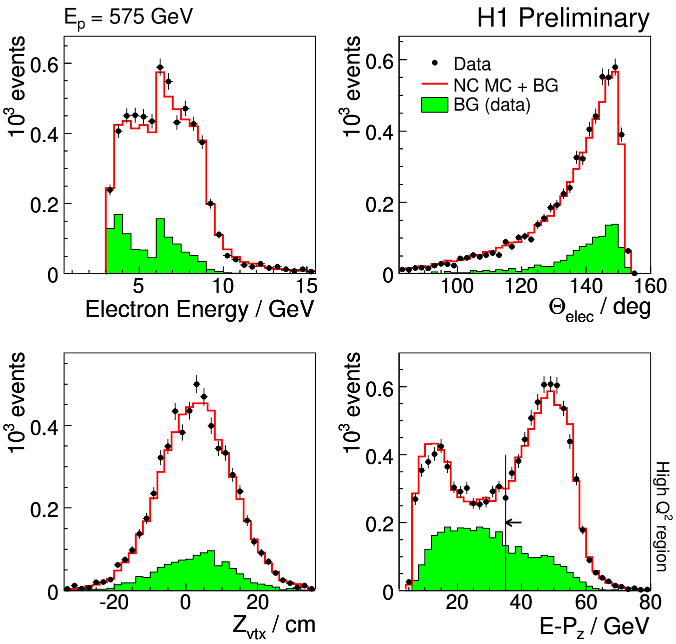

Figure 6: Comparison of the correct electron charge data (points) with a sum of background determined from the wrong “electron” charge data (green histogram) and DIS MC (open histogram) for the medium proton beam energy (575 GeV) in the high y range $0.7 < y < 0.9$. The distributions from left to right and from top to bottom are the scattered electron energy, the scattered electron polar angle Θ_{elec}, the z-position of the event vertex Z_{vtx} and the sum $E - p_z$ of all final state particles. The vertical line in $E - p_z$ distribution indicates the cut value.

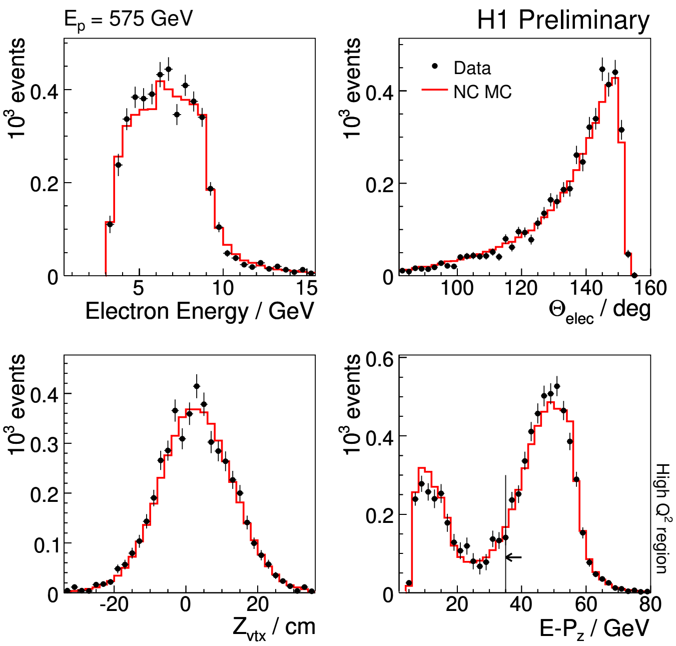

Figure 7: Comparison of signal distributions (background subtracted with corresponding asymmetry factor) for the medium proton beam energy (575 GeV) in the high y range $0.7 < y < 0.9$. The distributions from left to right and from top to bottom are the scattered electron energy, the scattered electron polar angle Θ_{elec}, the z-position of the event vertex Z_{vtx} and the sum $E - p_z$ of all final state particles. The vertical line in $E - p_z$ distribution indicates the cut value.

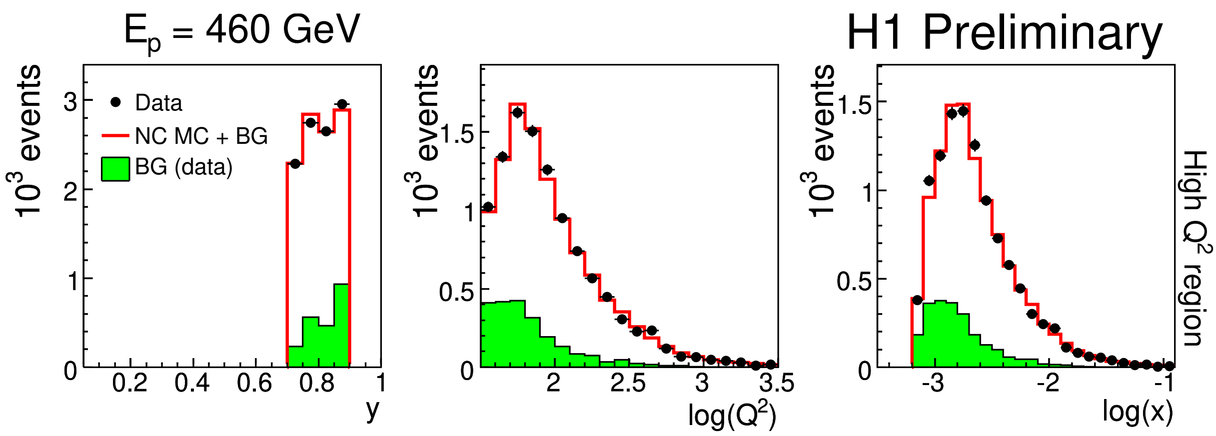

Figure 8: Comparison of the correct electron charge data (points) with a sum of background determined from the wrong "electron" charge data (green histogram) and DIS MC (open histogram) for the low proton beam energy (460 GeV) in the high y range $0.7 < y < 0.9$. The distributions from left to right are the inelasticity y, the four-momentum transfer squared Q^2 and Bjorken x.

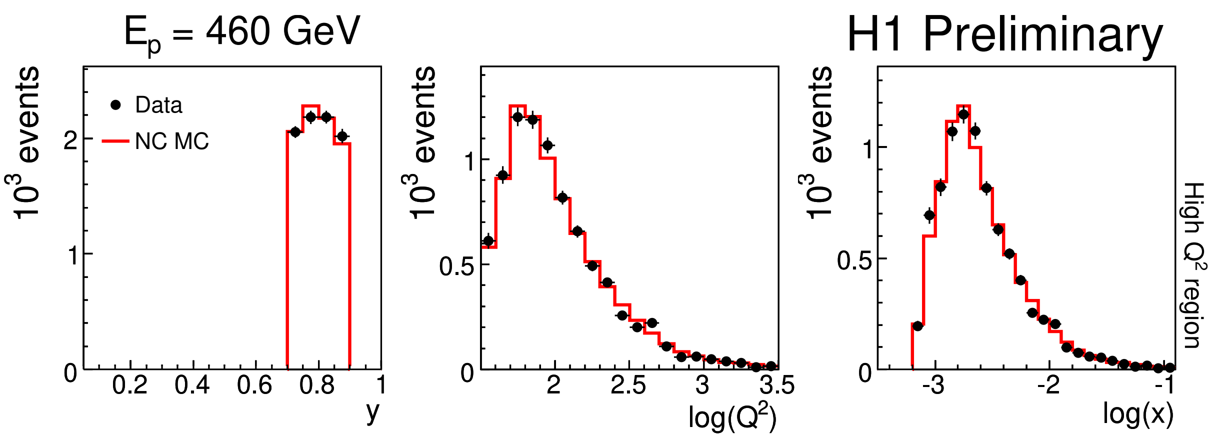

Figure 9: Comparison of signal distributions (background subtracted with corresponding asymmetry factor) for the low proton beam energy (460 GeV) in the high y range $0.7 < y < 0.9$. The distributions from left to right are the inelasticity y, the four-momentum transfer squared Q^2 and Bjorken x.

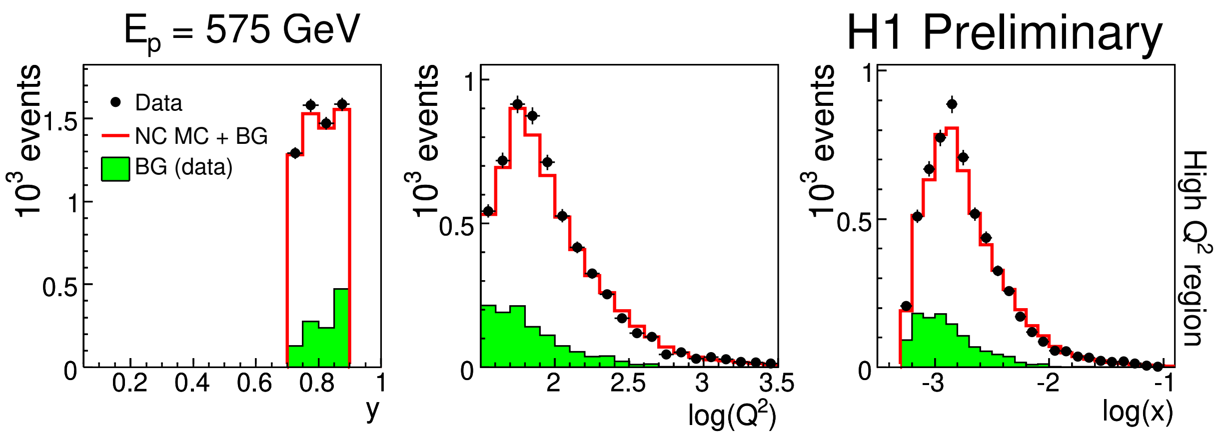

Figure 10: Comparison of the correct electron charge data (points) with a sum of background determined from the wrong "electron" charge data (green histogram) and DIS MC (open histogram) for the medium proton beam energy (575 GeV) in the high y range $0.7 < y < 0.9$. The distributions from left to right are the inelasticity y, the four-momentum transfer squared Q^2 and Bjorken x.

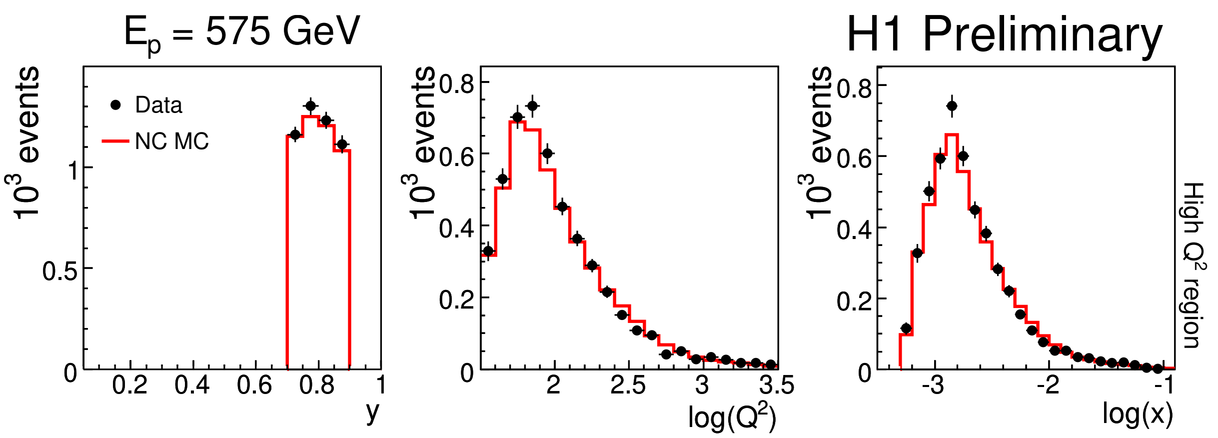

Figure 11: Comparison of signal distributions (background subtracted with corresponding asymmetry factor) for the medium proton beam energy (575 GeV) in the high y range $0.7 < y < 0.9$. The distributions from left to right are the inelasticity y, the four-momentum transfer squared Q^2 and Bjorken x.

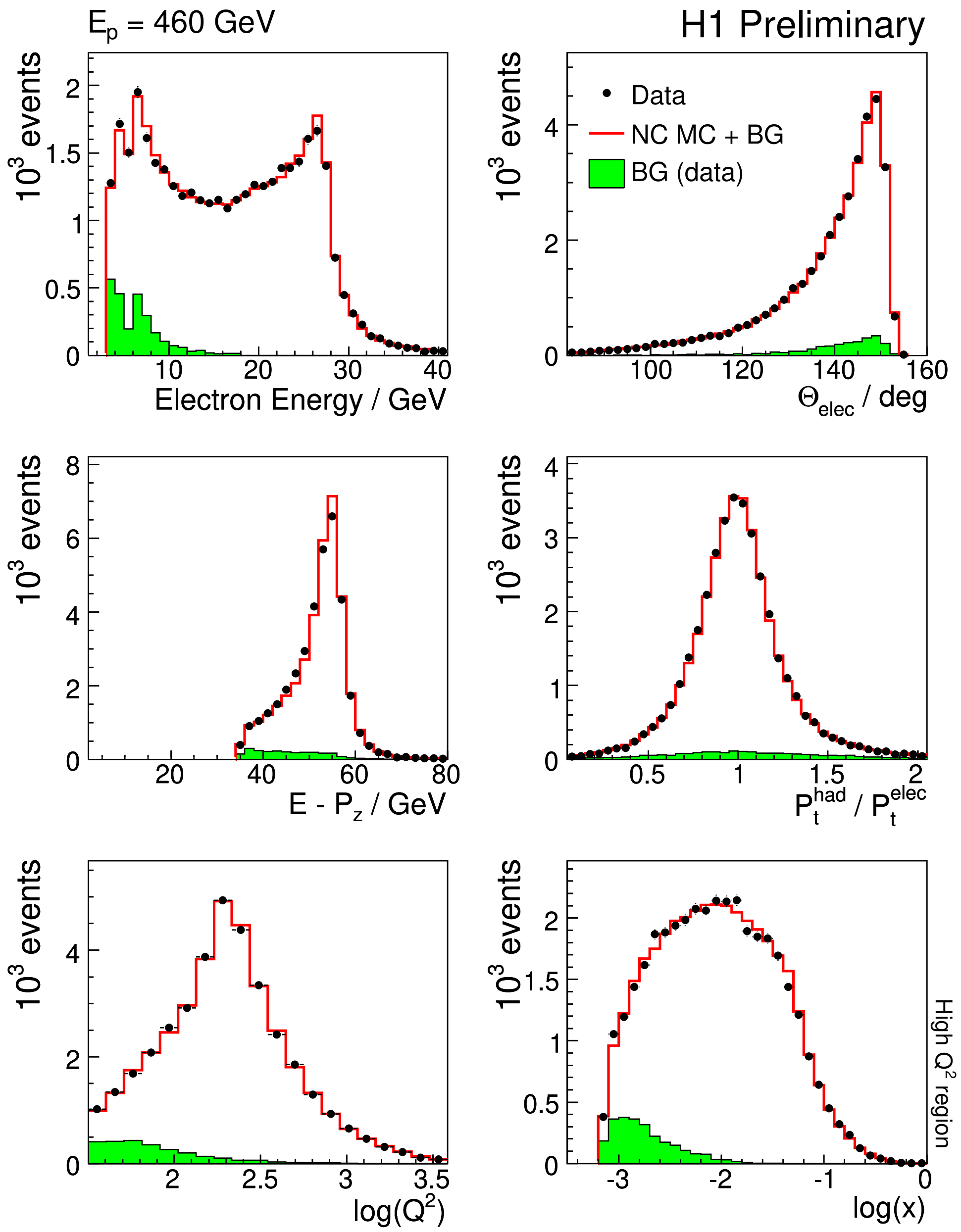

Figure 12: Comparison of the correct electron charge data (points) with a sum of background determined from the wrong "electron" charge data (green histogram) and DIS MC (open histogram) for the low proton beam energy (460 GeV) in the complete analysis range in y. The distributions from left to right and from top to bottom are the scattered electron energy, the scattered electron polar angle Θ_{elec}, the sum $E - p_z$ of all final state particles, momentum balance P_t^{had}/P_t^{elec}, the four-momentum transfer squared Q^2 and Bjorken x.

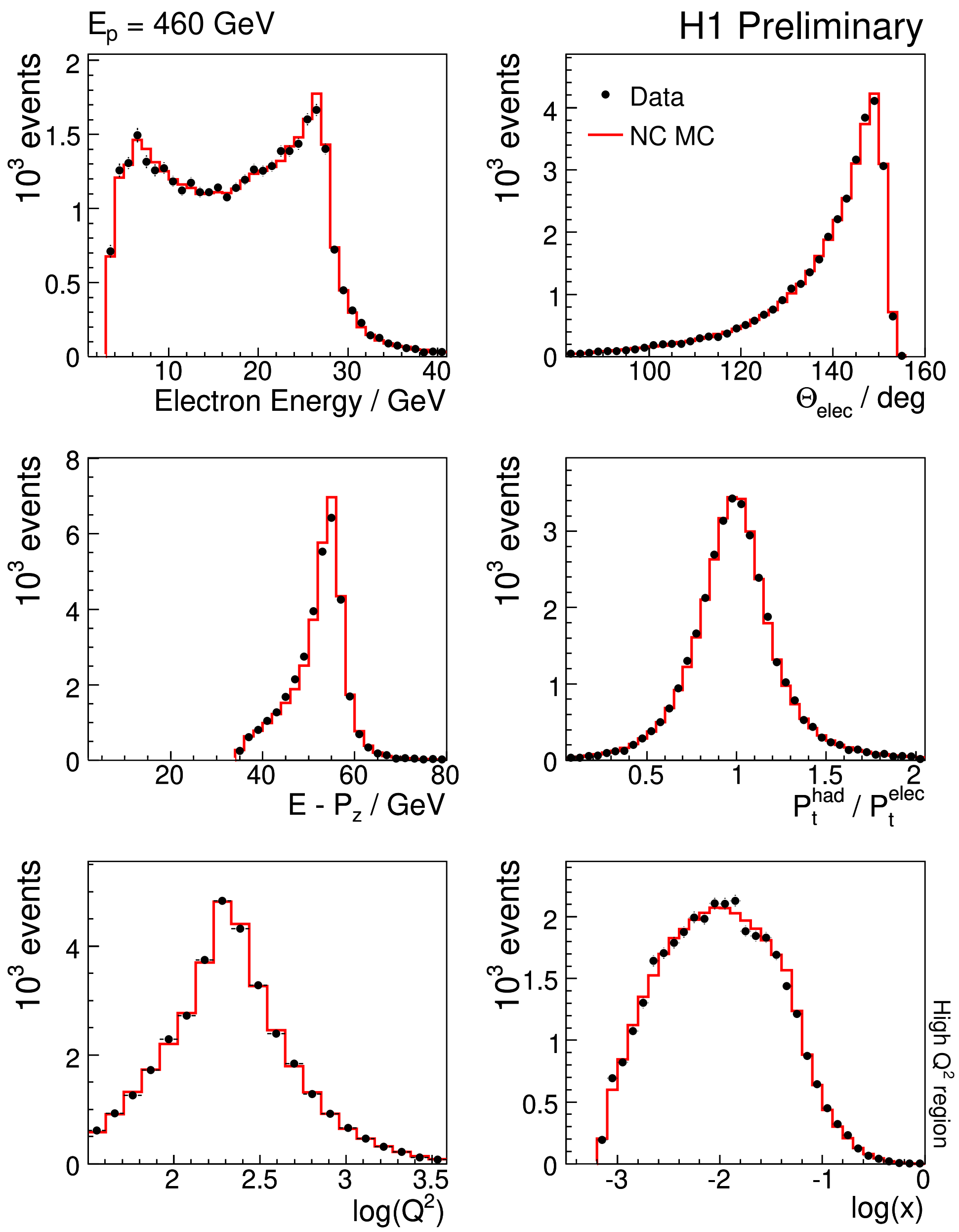

Figure 13: Comparison of signal distributions (background subtracted with corresponding asymmetry factor) for the low proton beam energy (460 GeV) in the complete analysis range in y. The distributions from left to right and from top to bottom are the scattered electron energy, the scattered electron polar angle Θ_{elec}, the sum $E - p_z$ of all final state particles, momentum balance P_t^{had}/P_t^{elec}, the four-momentum transfer squared Q^2 and Bjorken x.

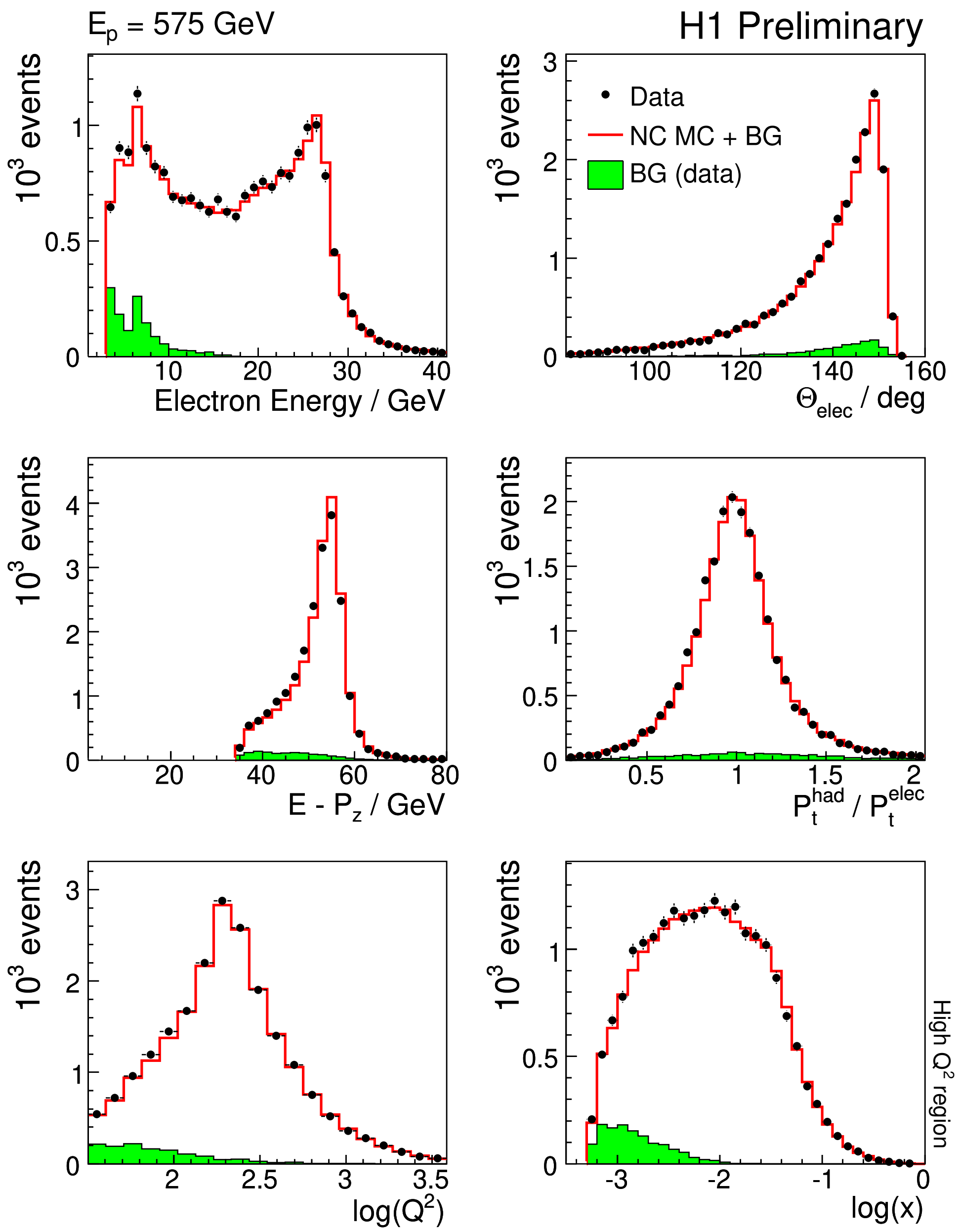

Figure 14: Comparison of the correct electron charge data (points) with a sum of background determined from the wrong "electron" charge data (green histogram) and DIS MC (open histogram) for the medium proton beam energy (575 GeV) in the complete analysis range in y. The distributions from left to right and from top to bottom are the scattered electron energy, the scattered electron polar angle Θ_{elec}, the sum $E - p_z$ of all final state particles, momentum balance P_t^{had}/P_t^{elec}, the four-momentum transfer squared Q^2 and Bjorken x.

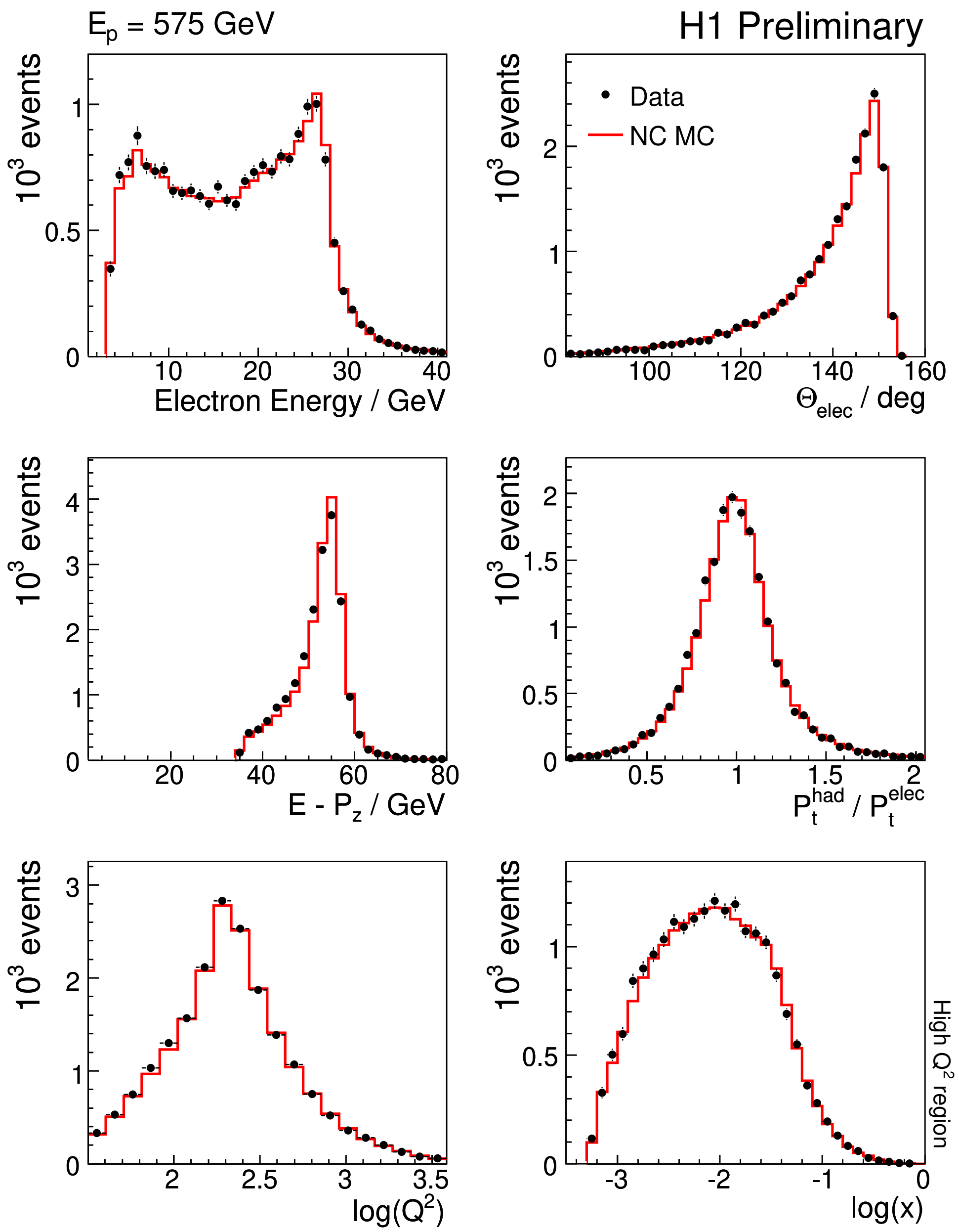

Figure 15: Comparison of signal distributions (background subtracted with corresponding asymmetry factor) for the medium proton beam energy (575 GeV) in the complete analysis range in y. The distributions from left to right and from top to bottom are the scattered electron energy, the scattered electron polar angle Θ_{elec}, the sum $E - p_z$ of all final state particles, momentum balance P_t^{had}/P_t^{elec}, the four-momentum transfer squared Q^2 and Bjorken x.

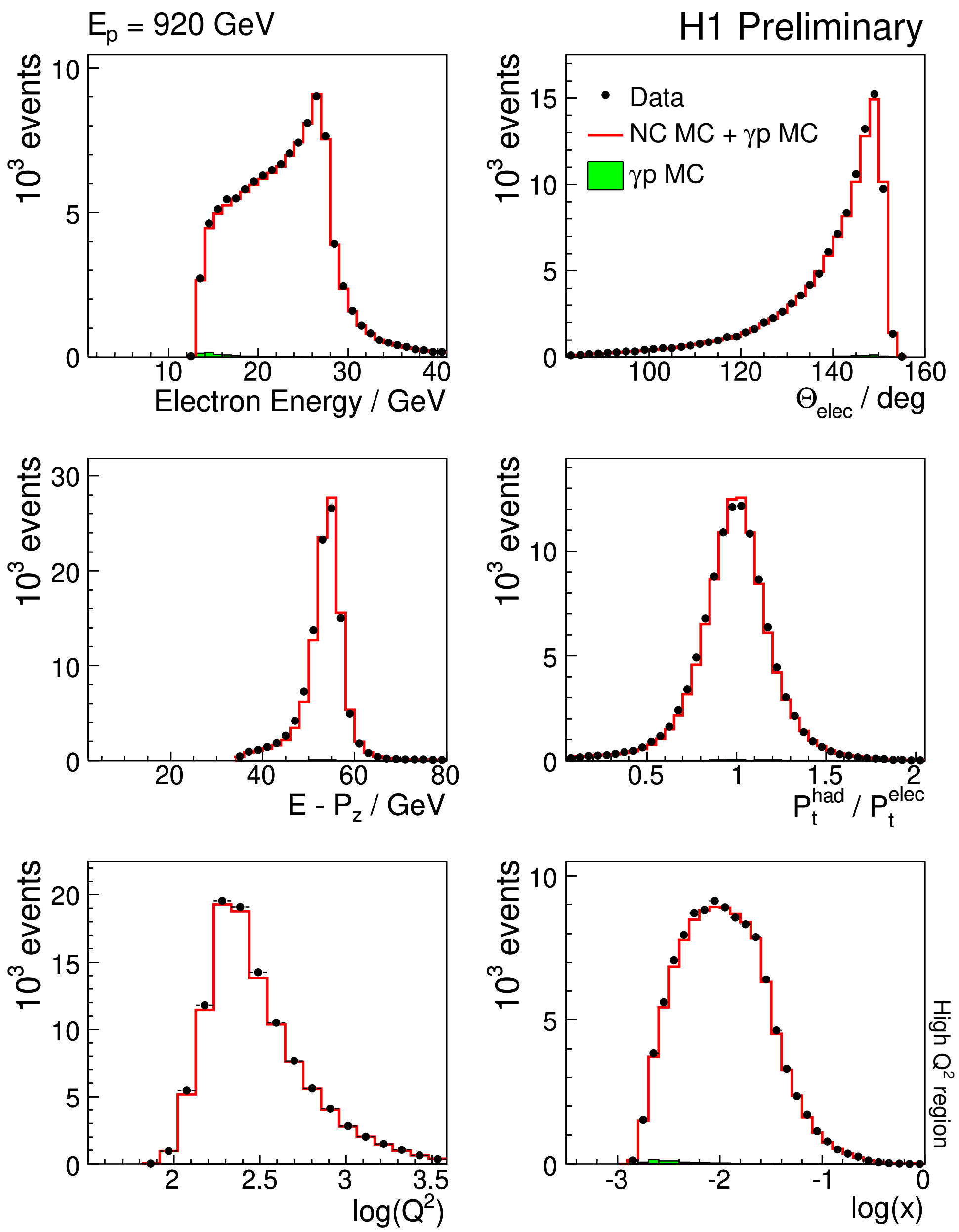

Figure 16: Comparison of the data (points) with a sum of background determined from photoproduction MC (green histogram) and DIS MC (open histogram) for the nominal proton beam energy (920 GeV) in the complete analysis range in y. The distributions from left to right and from top to bottom are the scattered electron energy, the scattered electron polar angle Θ_{elec}, the sum $E - p_z$ of all final state particles, momentum balance P_t^{had}/P_t^{elec}, the four-momentum transfer squared Q^2 and Bjorken x.

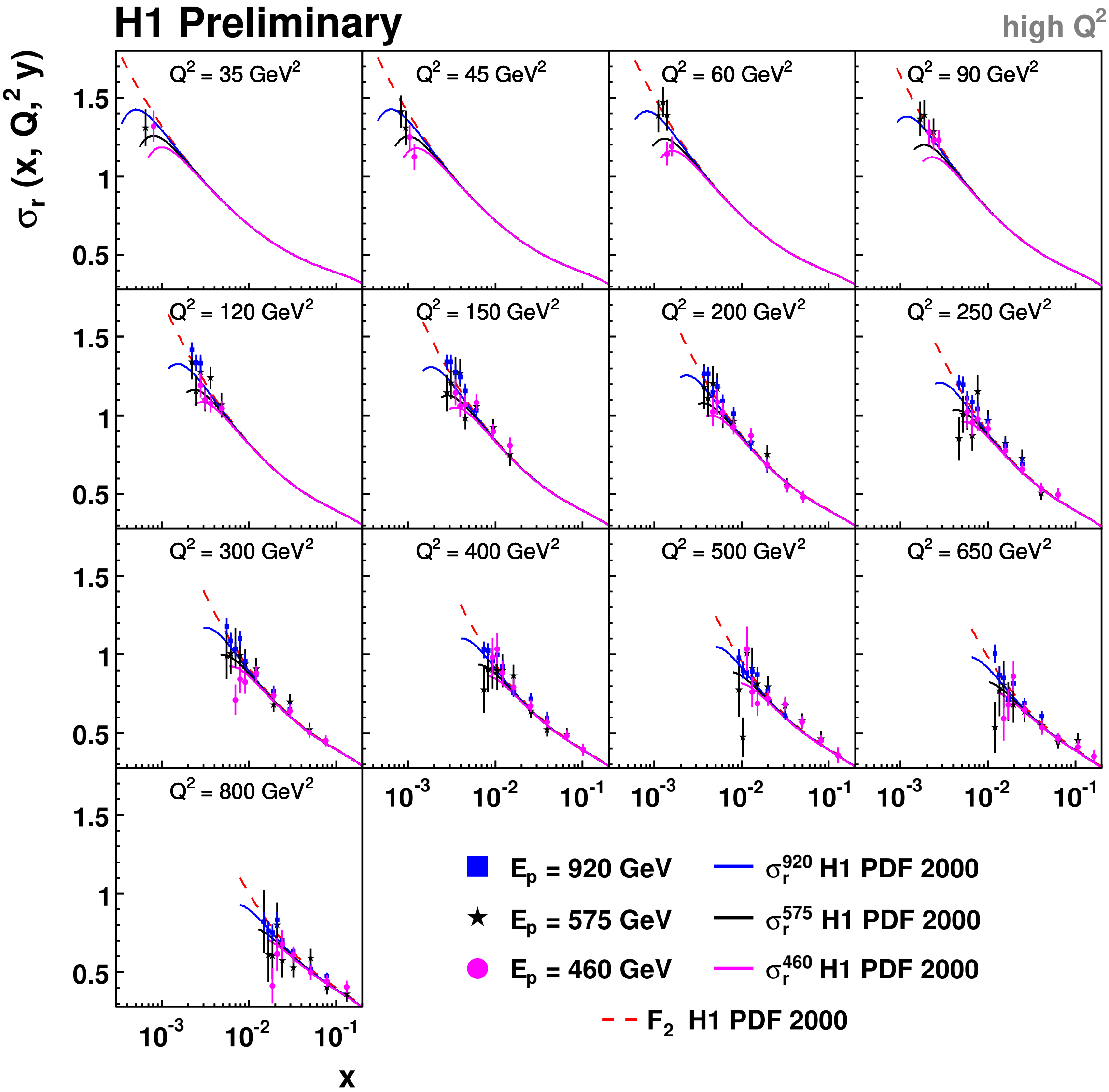

Figure 17: Reduced cross section measured at high Q^2 as a function of x using data taken at different proton beam energies of 920 GeV (full boxes), 575 GeV (stars) and 460 GeV (full points). The inner (outer) error bars represent statistical (total, with statistical and systematical errors added in quadrature) errors. Theoretical predictions of reduced cross section are shown as the solid lines for 920 GeV (blue), 575 GeV (black) and 460 GeV (red) line. The dashed line represents the QCD expectation of F_2. Theoretical expectations are derived from the H1 PDF 2000 fit.

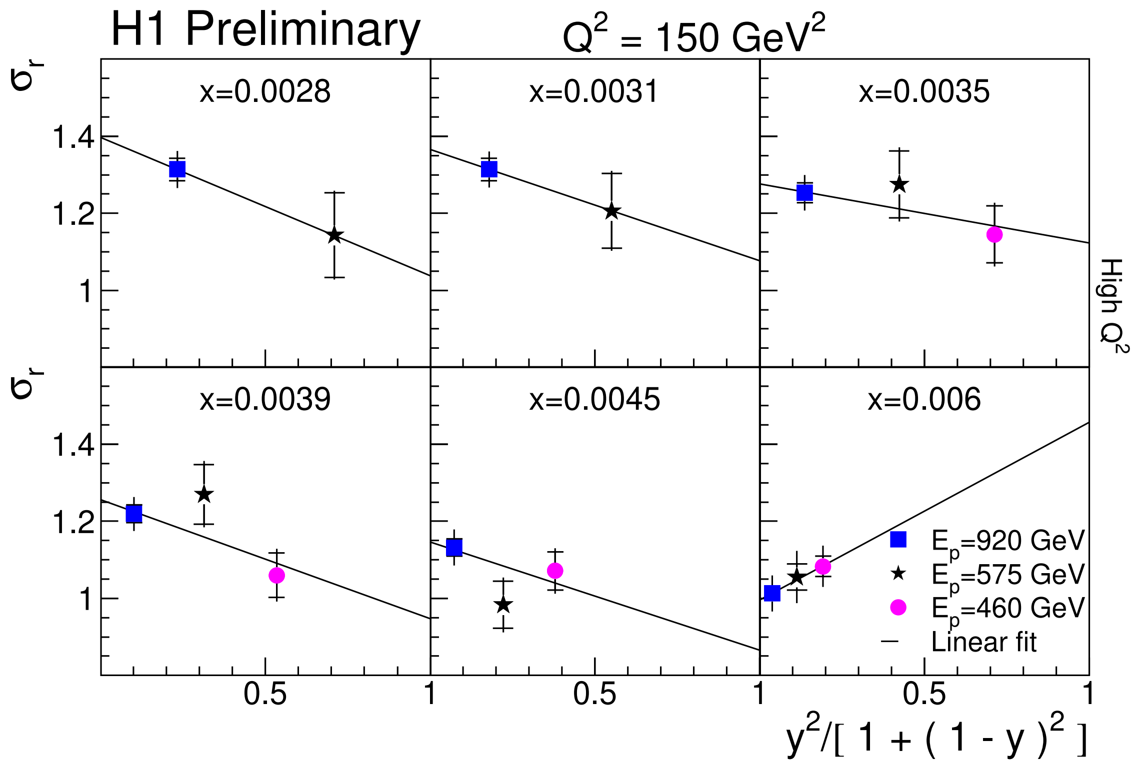

Figure 18: The reduced cross section $\sigma_r(x, Q^2, y)$ measured at $Q^2 = 150\ GeV^2$ and fixed values of x as a function of $f(y) = \frac{y^2}{1+(1-y)^2}$. The full boxes represent the nominal energy data (920 GeV), stars the medium energy data (575 GeV) and full circles the low energy data (460 GeV). The inner error bars are the statistical errors and the full error bars represent the statistical and systematic errors, added in quadrature. The lines show the linear fits used to determine F_L.

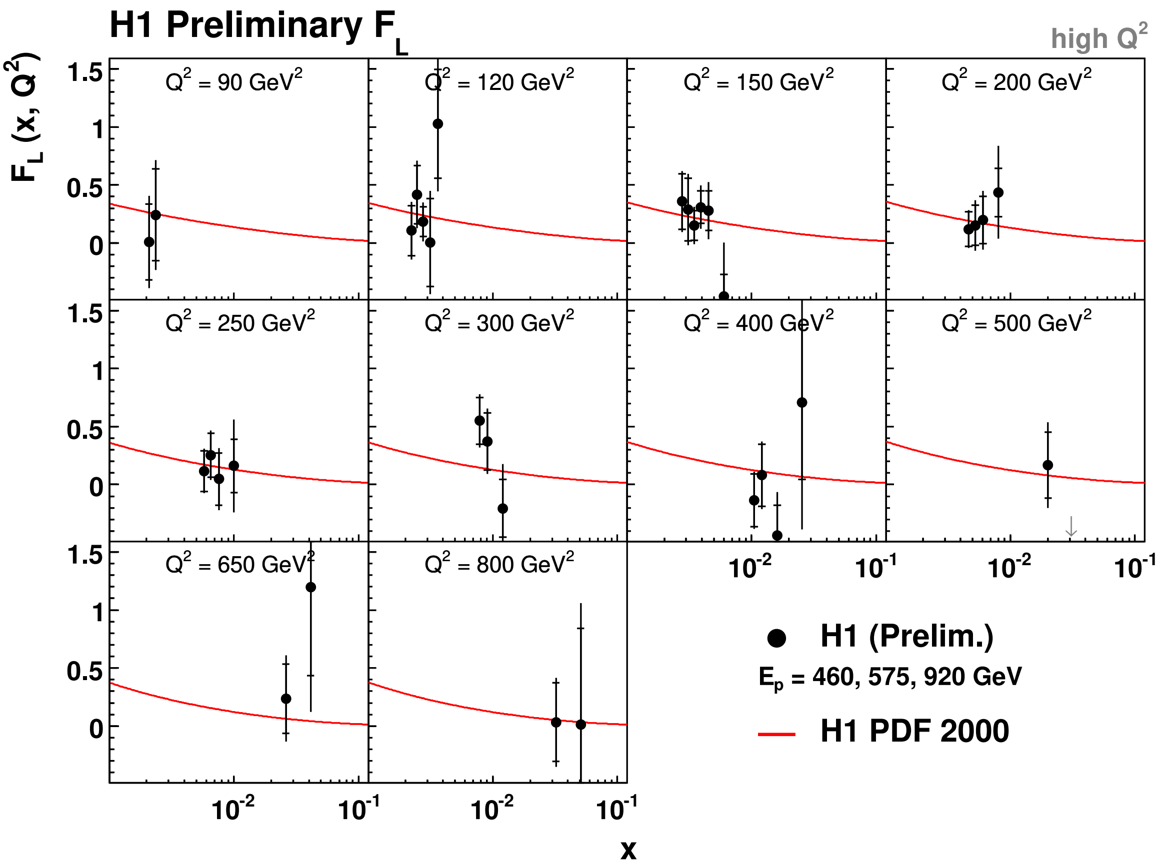

Figure 19: The longitudinal structure function F_L measured as a function of x at fixed values of Q^2 obtained from the LAr cross section measurements using data taken at different proton beam energies of 460 GeV, 575 GeV and 920 GeV. The inner error bars are the statistical errors and the full error bars represent the statistical and systematic errors, added in quadrature. The line represents a QCD prediction based on H1 PDF 2000 fit.

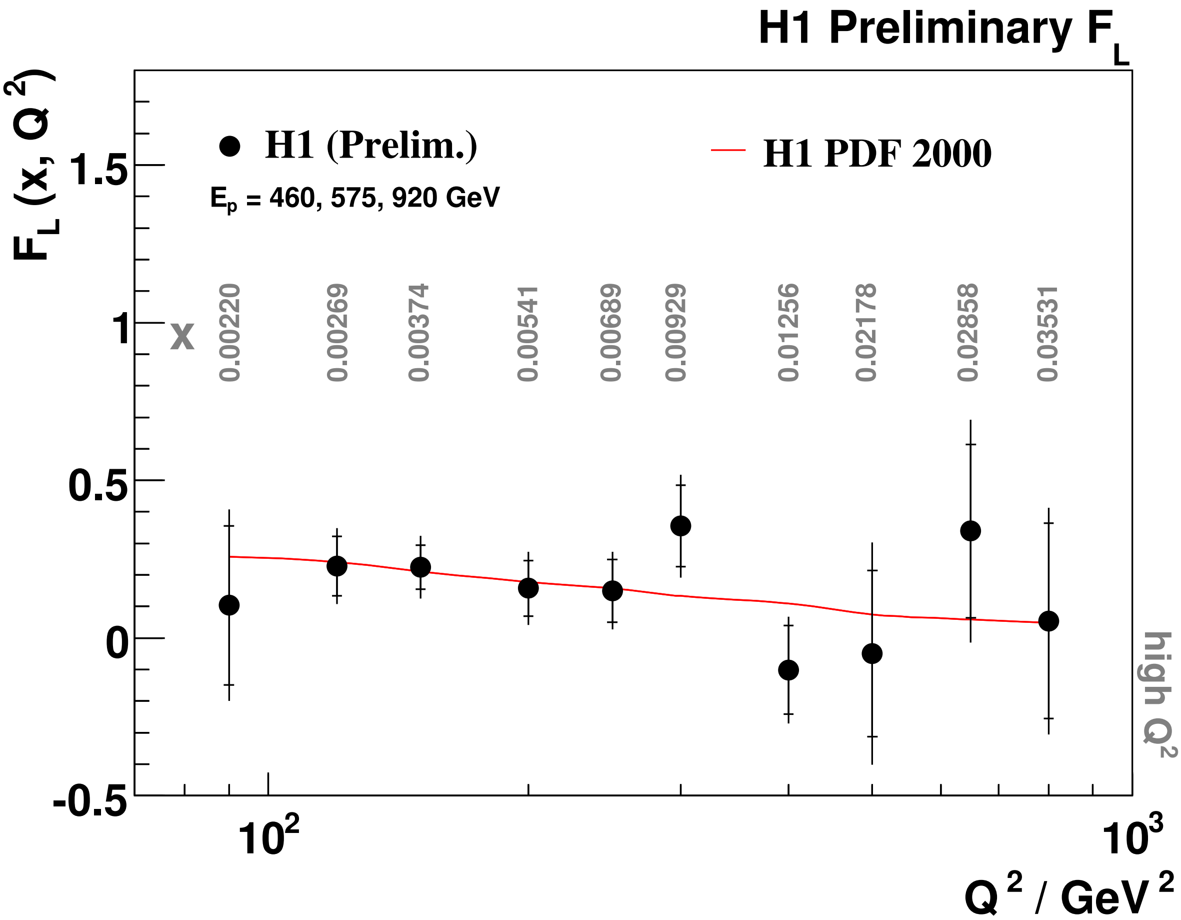

Figure 20: The longitudinal structure function F_L averaged in x at given value of Q^2 in the range of high Q^2 using data taken at different proton beam energies of 460 GeV, 575 GeV and 920 GeV. The resulting x values of the averaged F_L measurements are given in the figure for each point in Q^2. The inner error bars are the statistical errors and the full error bars represent the statistical and systematic errors, added in quadrature. The correlated systematic error between the averaged F_L measurements is estimated to vary between 0.05 and 0.10 in the measured kinematics range. The solid red line represents a QCD prediction based on H1 PDF 2000 fit.

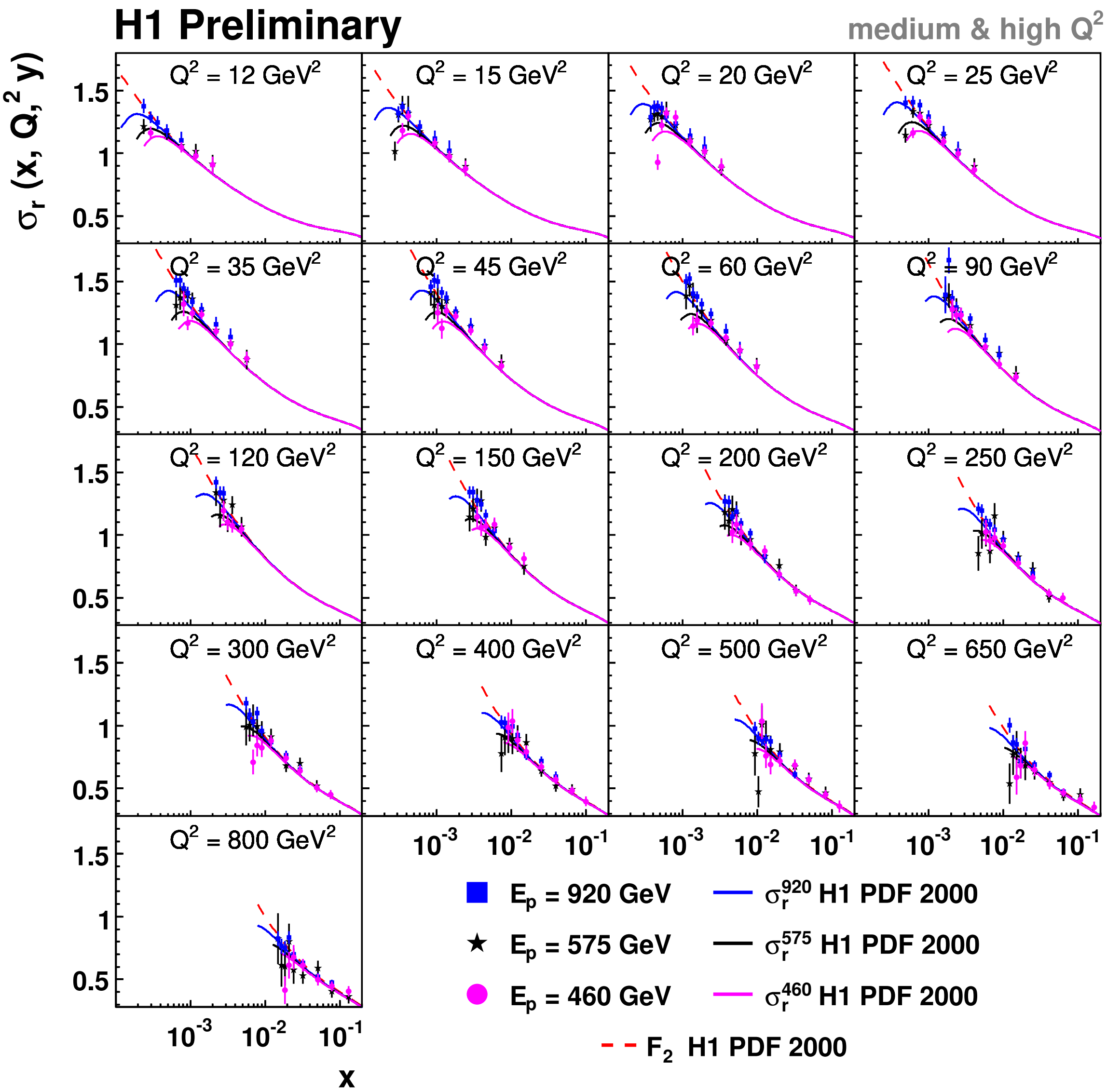

Figure 21: Reduced cross section measured in the full range of medium and high Q^2 as a function of x using data taken at different proton beam energies of 920 GeV (full boxes), 575 GeV (stars) and 460 GeV (full points). The inner (outer) error bars represent statistical (total, with statistical and systematical errors added in quadrature) errors. Theoretical predictions of reduced cross section are shown as the solid lines for 920 GeV (blue), 575 GeV (black) and 460 GeV (red) line. The dashed line represents the QCD expectation of F_2. Theoretical expectations are derived from the H1 PDF 2000 fit.

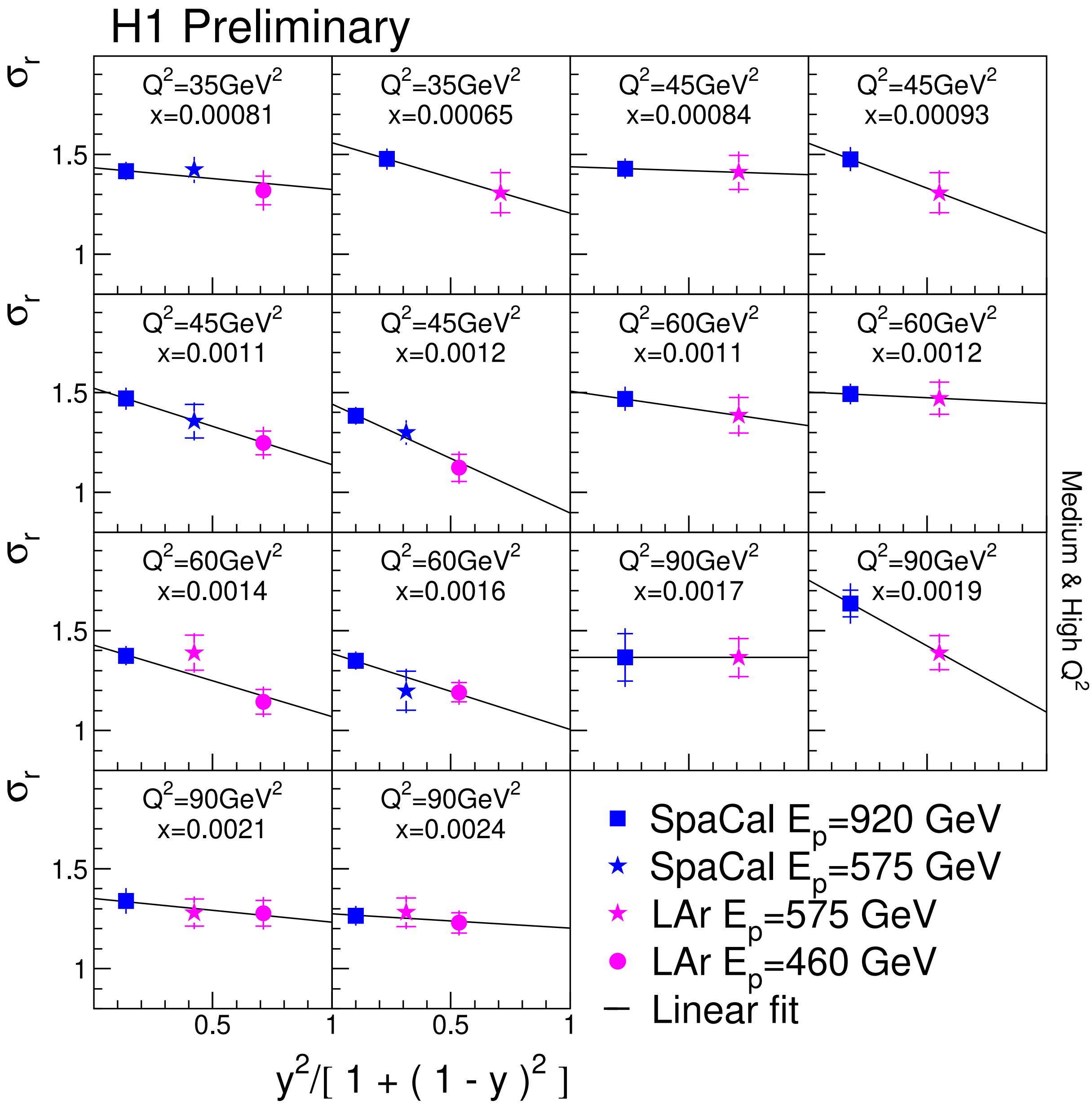

Figure 22: The reduced cross section $\sigma_r(x, Q^2, y)$ measured at fixed values of x and Q^2 as a function of $f(y) = \frac{y^2}{1+(1-y)^2}$. Only x and Q^2 values are shown which include cross section measurements from both LAr and Spacal analyses. The full boxes represent the nominal energy data (920 GeV), stars the medium energy data (575 GeV) and full circles the low energy data (460 GeV). The inner error bars are the statistical errors and the full error bars represent the statistical and systematic errors, added in quadrature. The lines show the linear fits used to determine F_L.

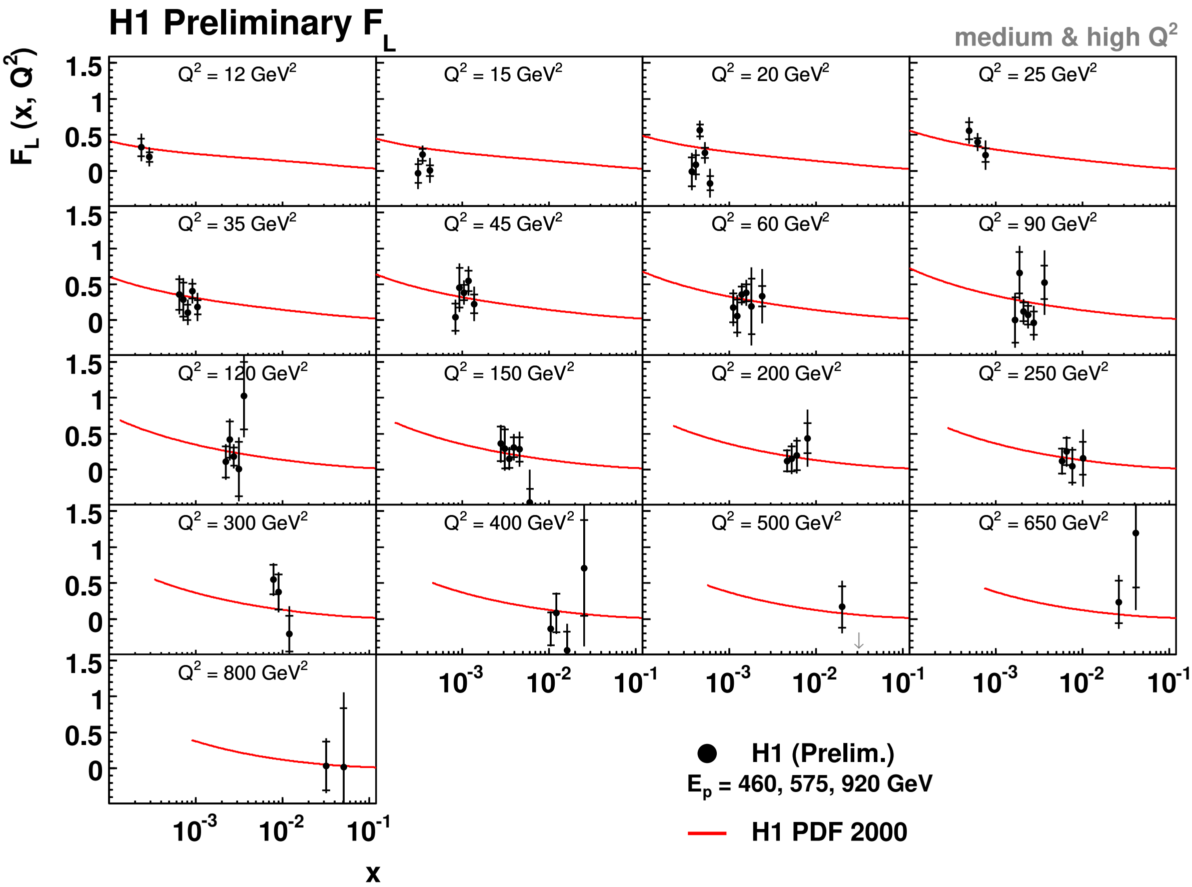

Figure 23: The longitudinal structure function F_L measured as a function of x at fixed values of Q^2 in the full range of medium and high Q^2 using data taken at different proton beam energies of 460 GeV, 575 GeV and 920 GeV. The inner error bars are the statistical errors and the full error bars represent the statistical and systematic errors, added in quadrature. The line represents a QCD prediction based on H1 PDF 2000 fit.

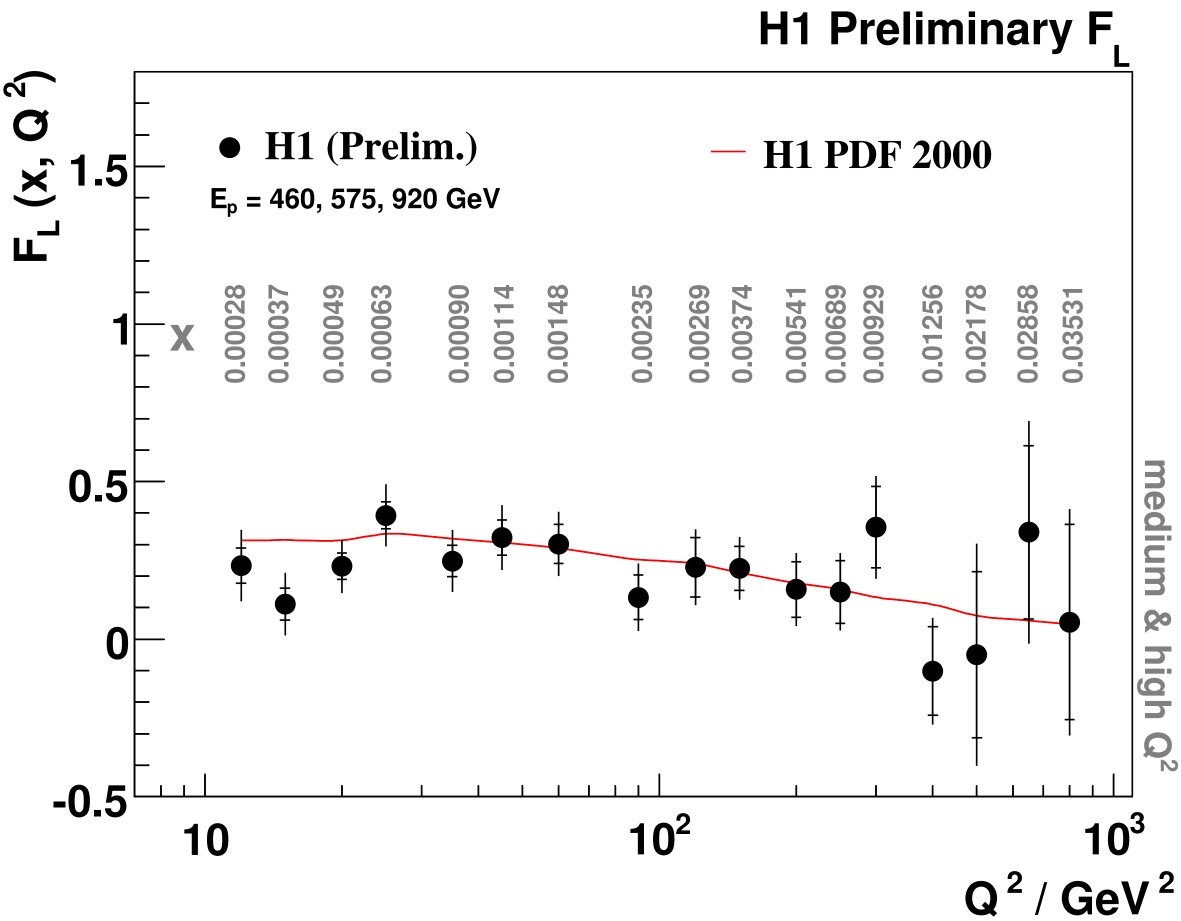

Figure 24: The longitudinal structure function F_L averaged in x at given value of Q^2 in the full range of medium and high Q^2 using data taken at different proton beam energies of 460 GeV, 575 GeV and 920 GeV. The resulting x values of the averaged F_L measurements are given in the figure for each point in Q^2. The inner error bars are the statistical errors and the full error bars represent the statistical and systematic errors, added in quadrature. The correlated systematic error between the averaged F_L measurements is estimated to vary between 0.05 and 0.10 in the measured kinematics range. The solid red line represents a QCD prediction based on H1 PDF 2000 fit.

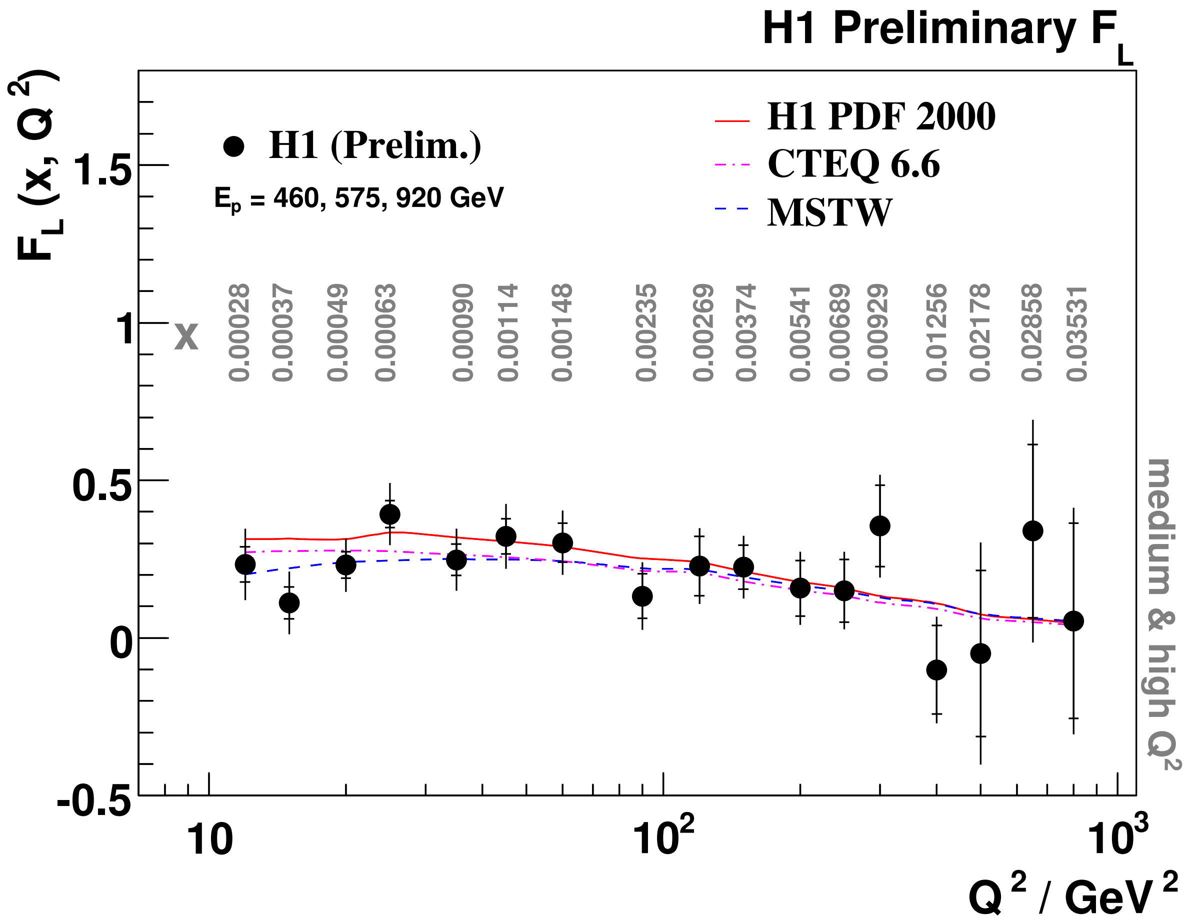

Figure 25: The longitudinal structure function F_L averaged in x at given value of Q^2 in the full range of medium and high Q^2 using data taken at different proton beam energies of 460 GeV, 575 GeV and 920 GeV. The resulting x values of the averaged F_L measurements are given in the figure for each point in Q^2. The inner error bars are the statistical errors and the full error bars represent the statistical and systematic errors, added in quadrature. The correlated systematic error between the averaged F_L measurements is estimated to vary between 0.05 and 0.10 in the measured kinematics range. The solid red line represents a QCD prediction based on H1 PDF 2000 fit. The dashed lines represents the MSTW and the dashed-dotted line the CTEQ6.6 predictions (private communications).

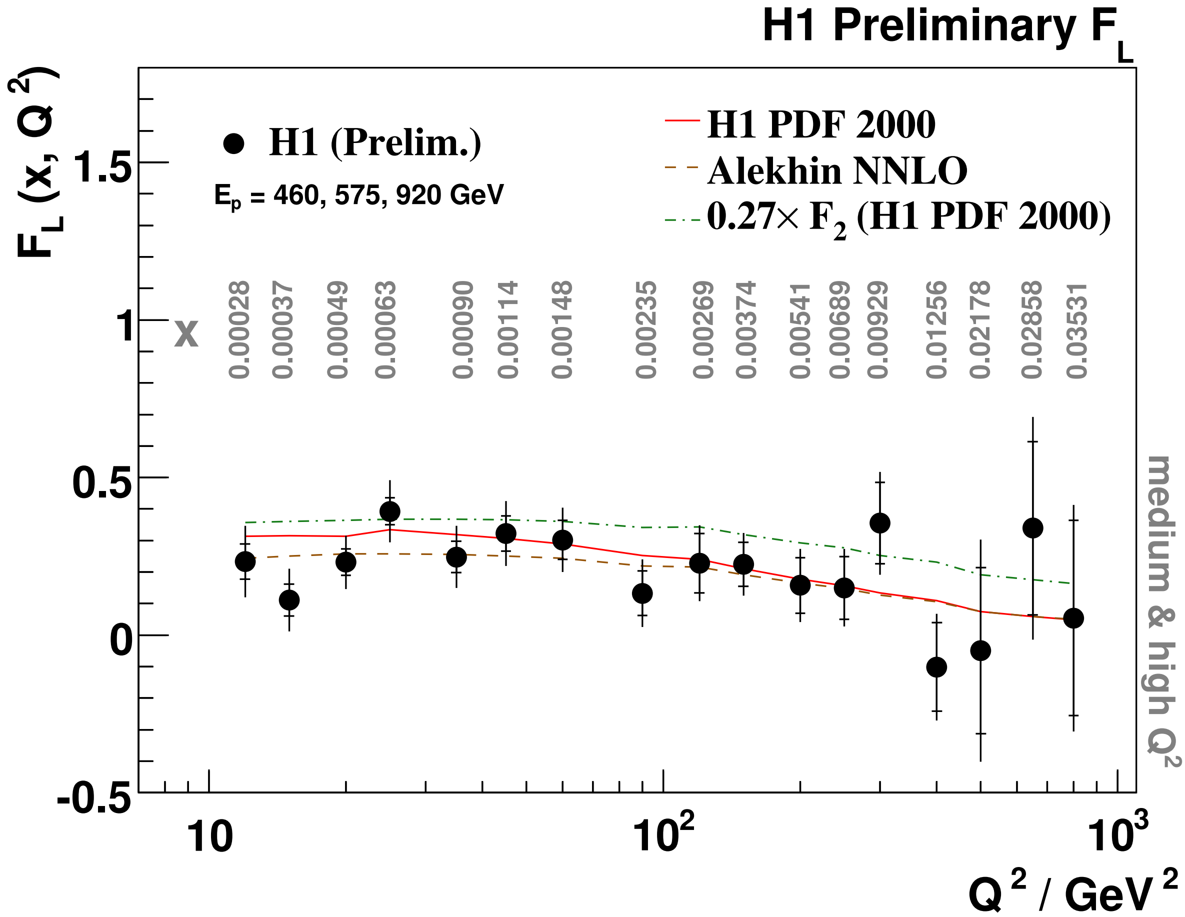

Figure 26: The longitudinal structure function F_L averaged in x at given value of Q^2 in the full range of medium and high Q^2 using data taken at different proton beam energies of 460 GeV, 575 GeV and 920 GeV. The resulting x values of the averaged F_L measurements are given in the figure for each point in Q^2. The inner error bars are the statistical errors and the full error bars represent the statistical and systematic errors, added in quadrature. The correlated systematic error between the averaged F_L measurements is estimated to vary between 0.05 and 0.10 in the measured kinematics range. The solid red line represents a QCD prediction based on H1 PDF 2000 fit. The dashed brown line represents FL calculations based on the NNLO QCD fit by S. Alekhin (Phys.Rev.D74:054033,2006) and the green dashed-dotted line corresponds to 0.27 times F2 from the H1 PDF 2000 fit, motivated by the recent publication of M. Kuroda and D. Schildknecht (arXiv:0806:0202).